Electronic Supplementary Information

Electrostatic Self-Assembly of AgI/$Bi_2Ga_4O_9$ p-n Junction Photocatalyst for Boosting Superoxide Radical Generation

Jin Liu,[a] Xingcai Zhang,[b] Qian Zhong,[a] Jun Li,*[c] Hongzhang Wu,[a] Bo Zhang,[a] Lin Jin,*[a] Hua Bing Tao,*[d] and Bin Liu*[d]

[a] *Henan Key Laboratory of Rare Earth Functional Materials, International Joint Research Laboratory for Biomedical Nanomaterials of Henan, Zhoukou Normal University, Zhoukou 466001, P. R. China*

[b] *John A. Paulson School of Engineering and Applied Sciences, Harvard University, Cambridge, MA, 02138, United States*

[c] *Henan Institute of Advanced Technology, Zhengzhou University, Zhengzhou 450001, P. R. China*

[d] *School of Chemical and Biomedical Engineering, Nanyang Technological University, 62 Nanyang Drive, Singapore 637459, Singapore*

**Corresponding author, E-mail address: junlee1992@126.com (Jun Li), jinlin_1982@126.com (Lin Jin), hbtao@ntu.edu.sg (Hua Bing Tao), liubin@ntu.edu.sg (Bin Liu)*

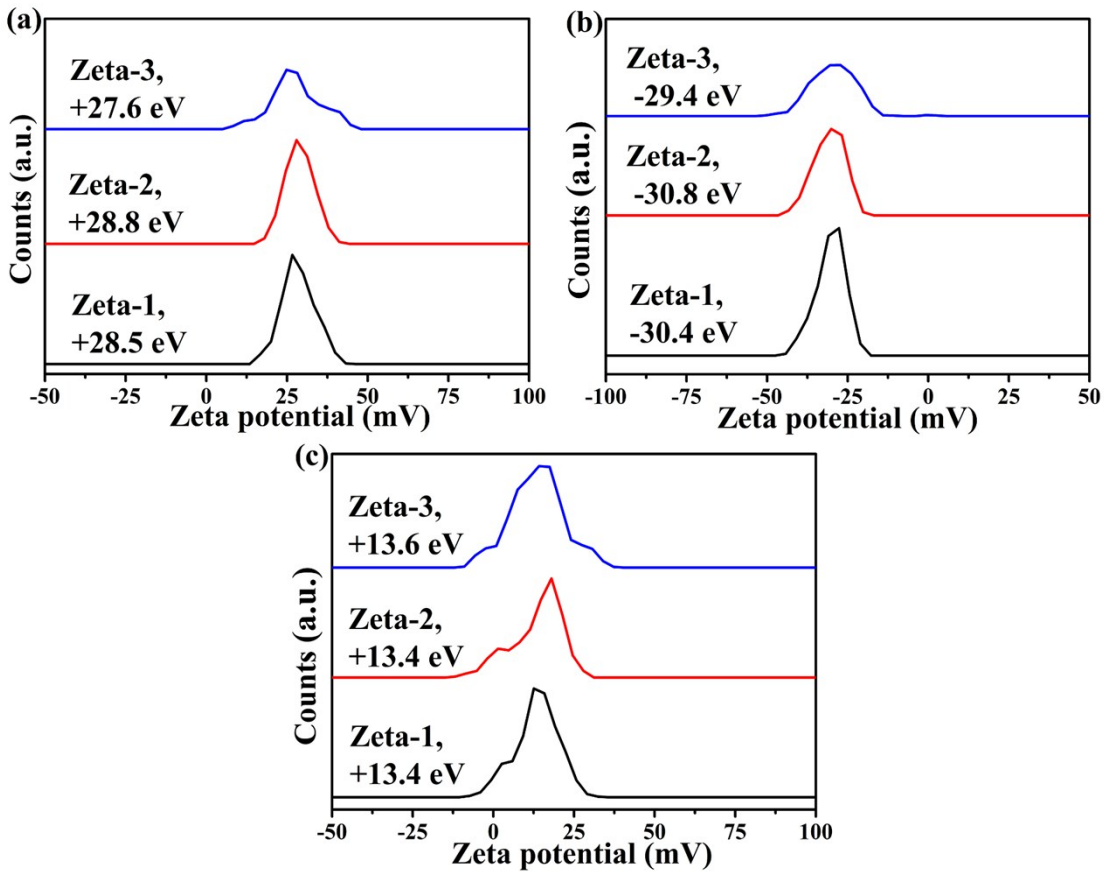

Fig. S1 Zeta potential of (a) $Bi_2Ga_4O_9$, (b) AgI and (c) 25%-AgI/ $Bi_2Ga_4O_9$. Zeta-1, Zeta-2, and Zeta-3 represent the first, second and third time measurement results, respectively.

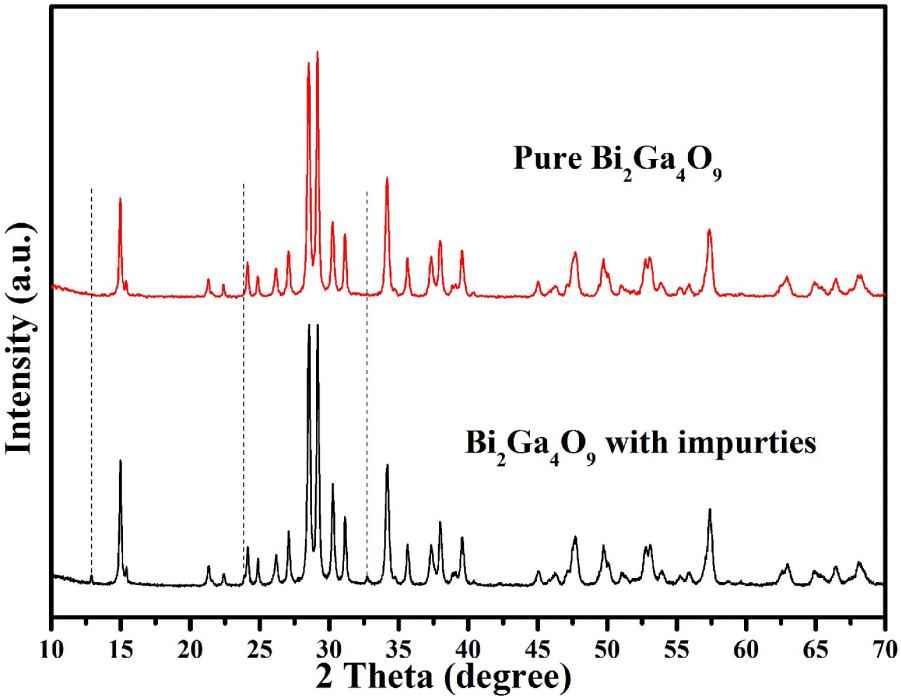

Fig. S2 XRD patterns of $Bi_2Ga_4O_9$ with impurities and pure $Bi_2Ga_4O_9$.

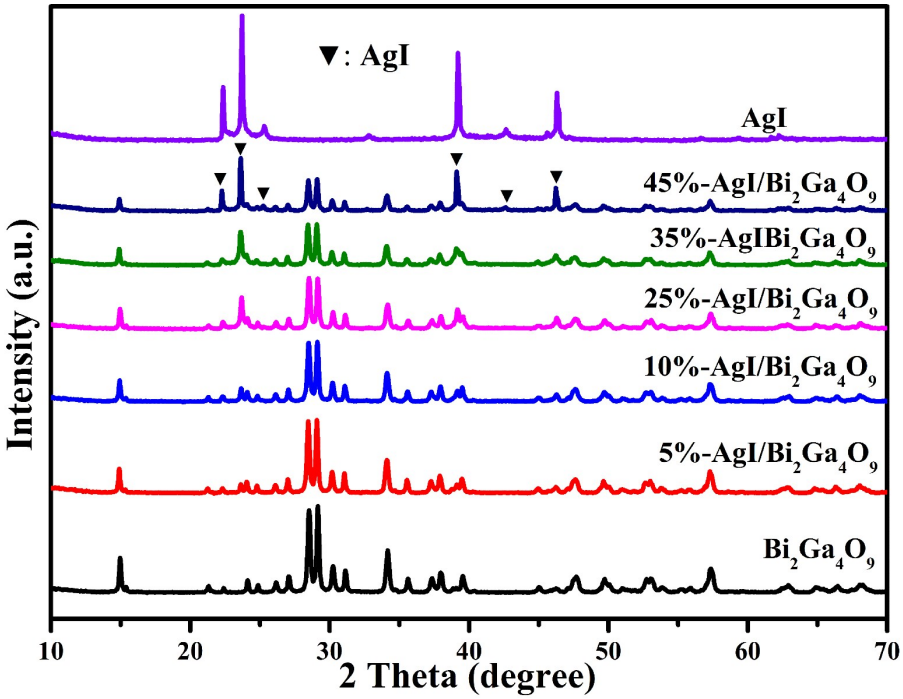

Fig. S3 XRD patterns of $Bi_2Ga_4O_9$, AgI and AgI/$Bi_2Ga_4O_9$ samples.

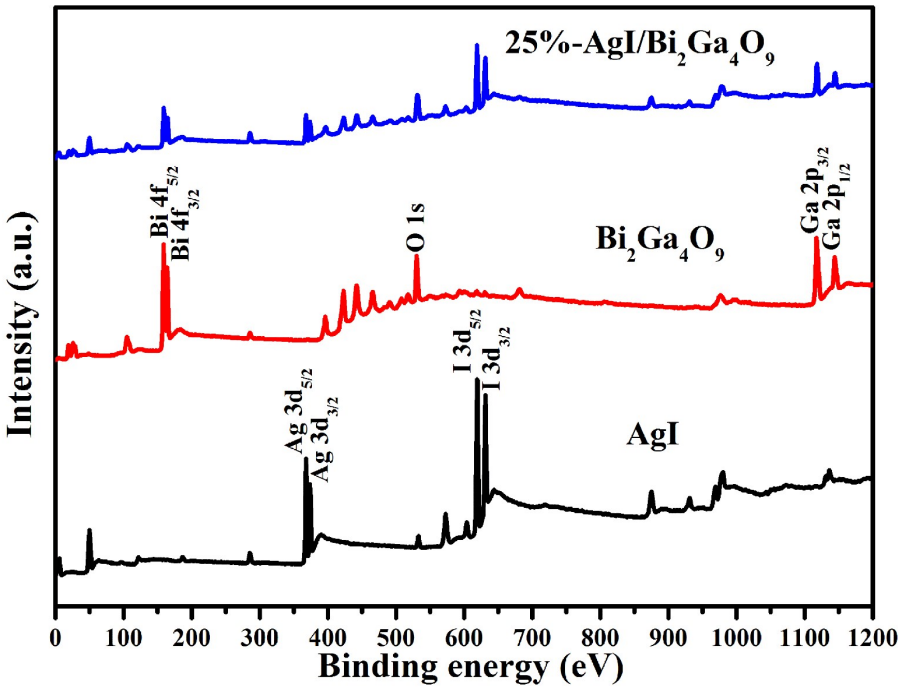

Fig. S4 XPS survey spectra.

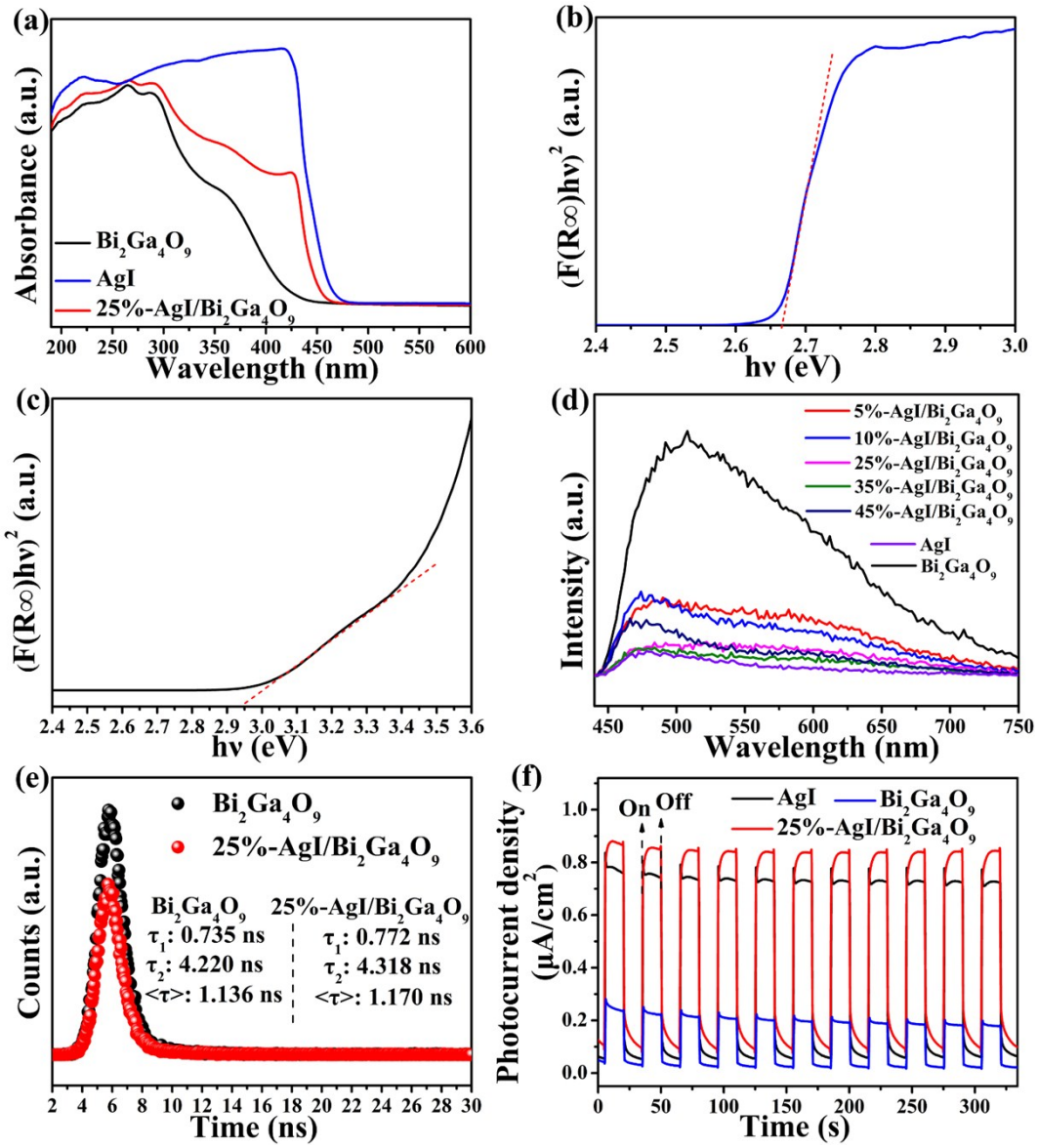

Fig. S5 (a) UV-vis absorption spectra. (b) Plot of $(F(R_\infty)h\nu)^2$ vs. photon energy for AgI. (c) Plot of $(F(R_\infty))^{1/2}$ vs. photon energy for $Bi_2Ga_4O_9$. (d) PL spectra, (e) time-resolved PL decay curves, and (f) change of photocurrent density with time.

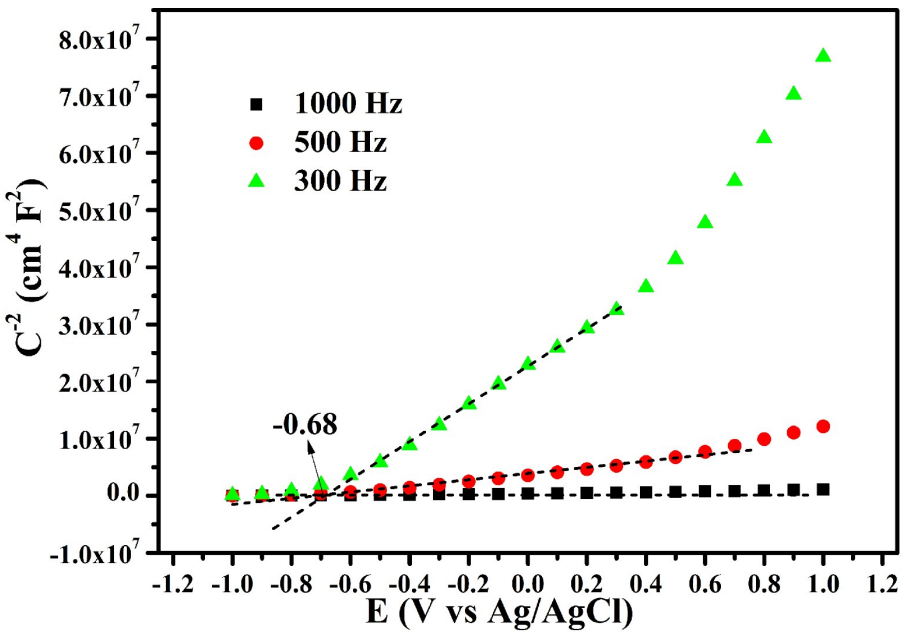

Fig. S6 Mott-Schottky plots of $Bi_2Ga_4O_9$.

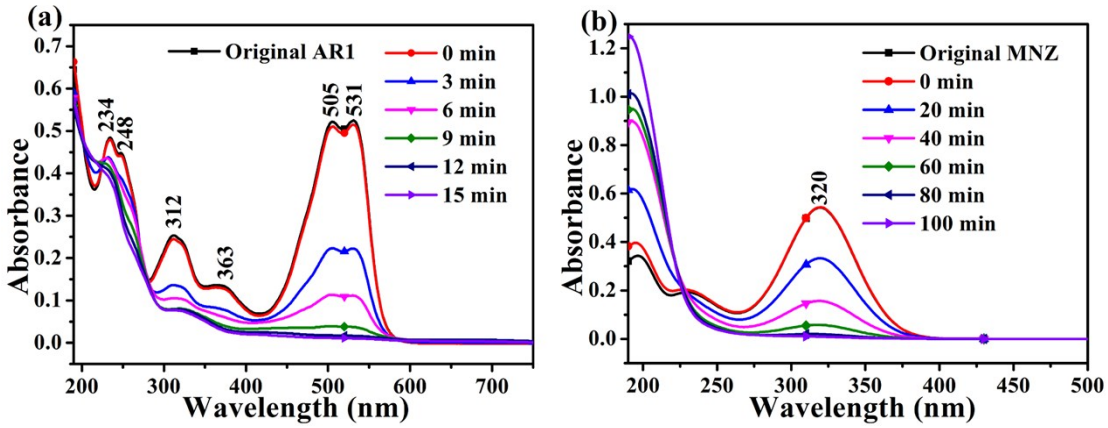

Fig. S7 UV-vis absorption spectra of (a) AR1 and (b) MNZ recorded after different durations of irradiation over 25%-AgI/$Bi_2Ga_4O_9$.

(a)

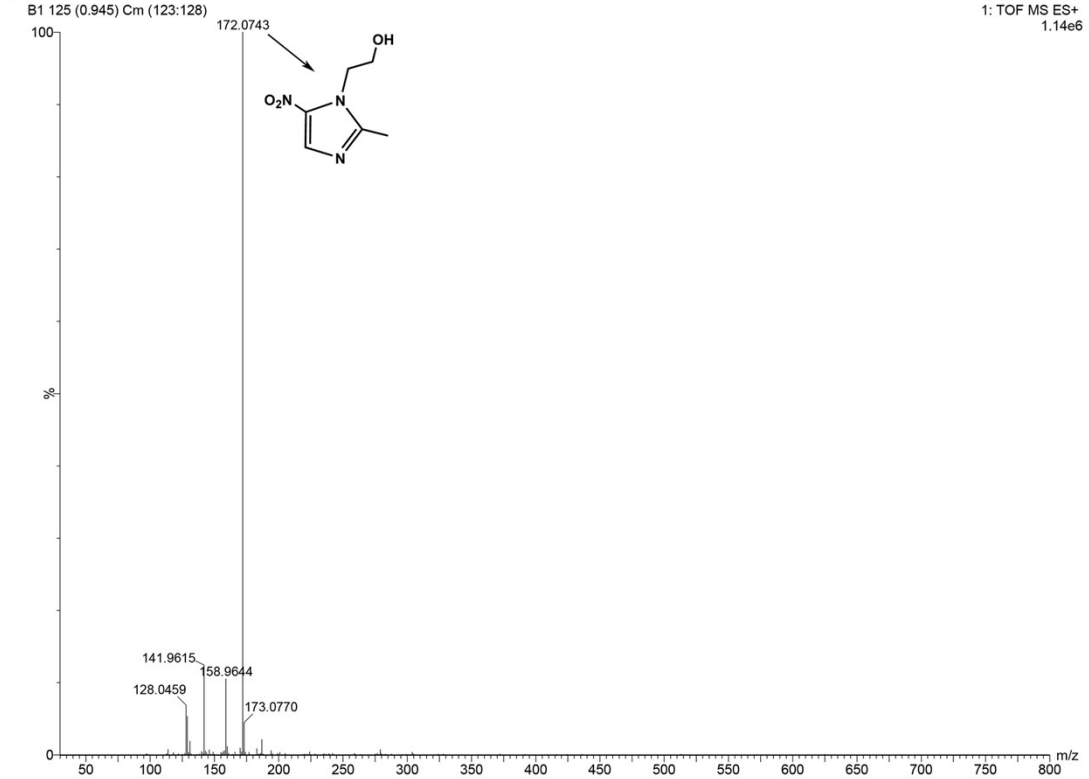
B1 125 (0.945) Cm (123:128)
1: TOF MS ES+
1.14e6
172.0743
141.9615
158.9644
128.0459
173.0770
m/z

(b)

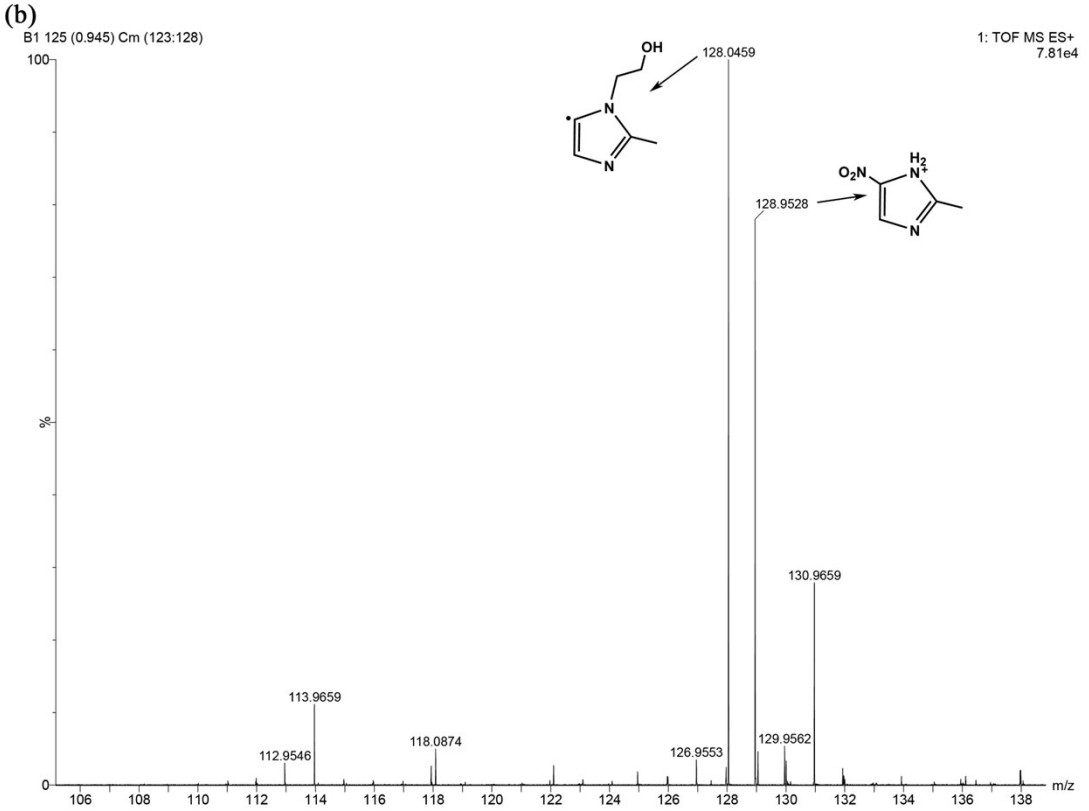
B1 125 (0.945) Cm (123:128)
1: TOF MS ES+
7.81e4
128.0459
128.9528
130.9659
113.9659
112.9546
118.0874
126.9553
129.9562
m/z

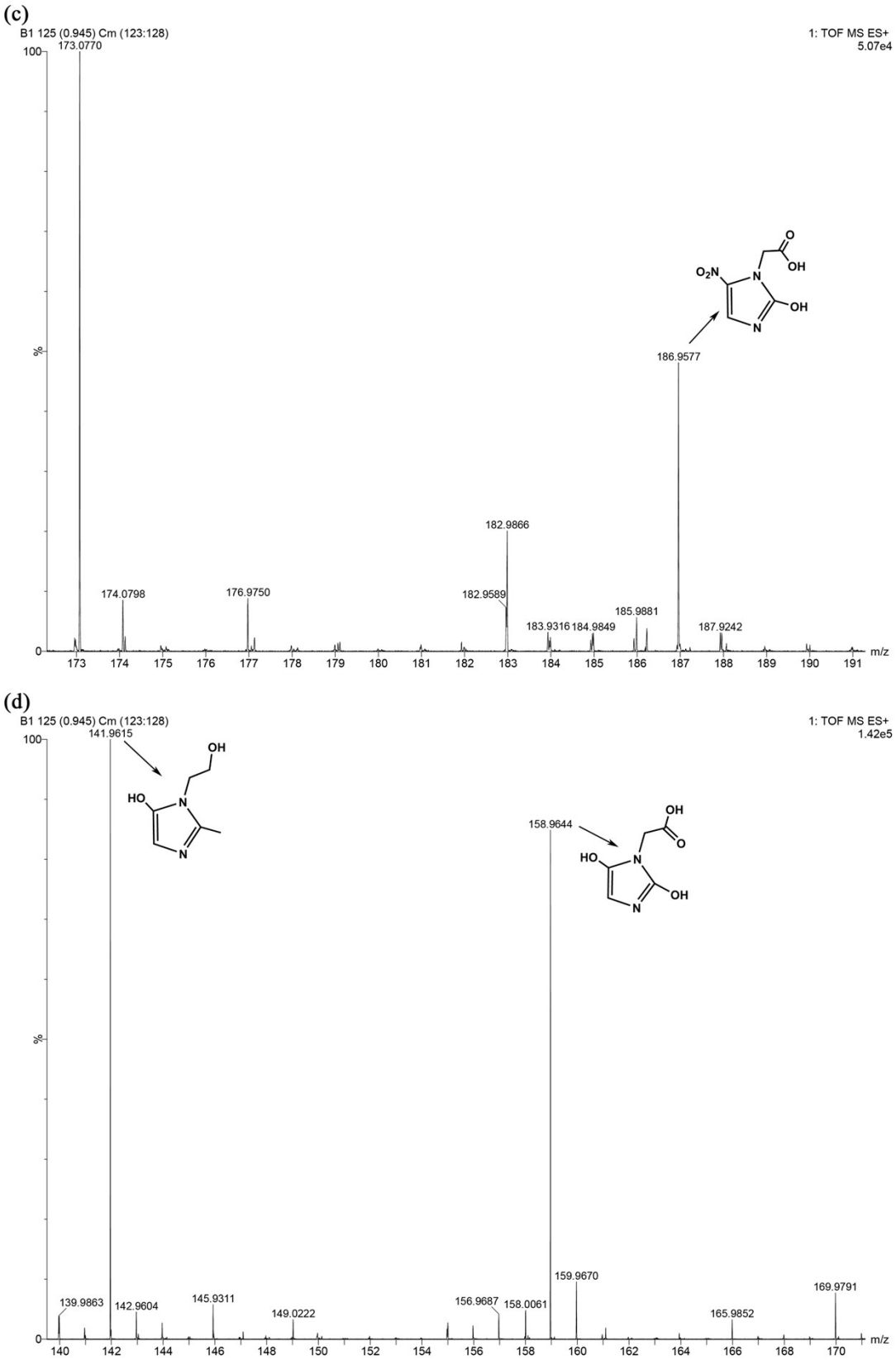

Fig. S8 Mass spectra and molecular structures of the intermediates in the photocatalytic degradation of MNZ over 25%-AgI/$Bi_2Ga_4O_9$.

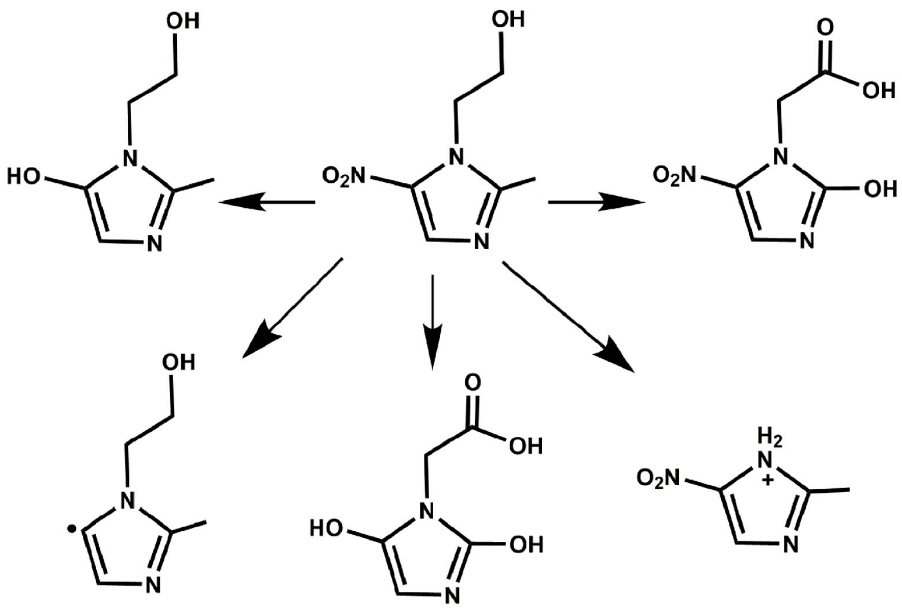

Fig. S9 Possible photocatalytic degradation pathways of MNZ.

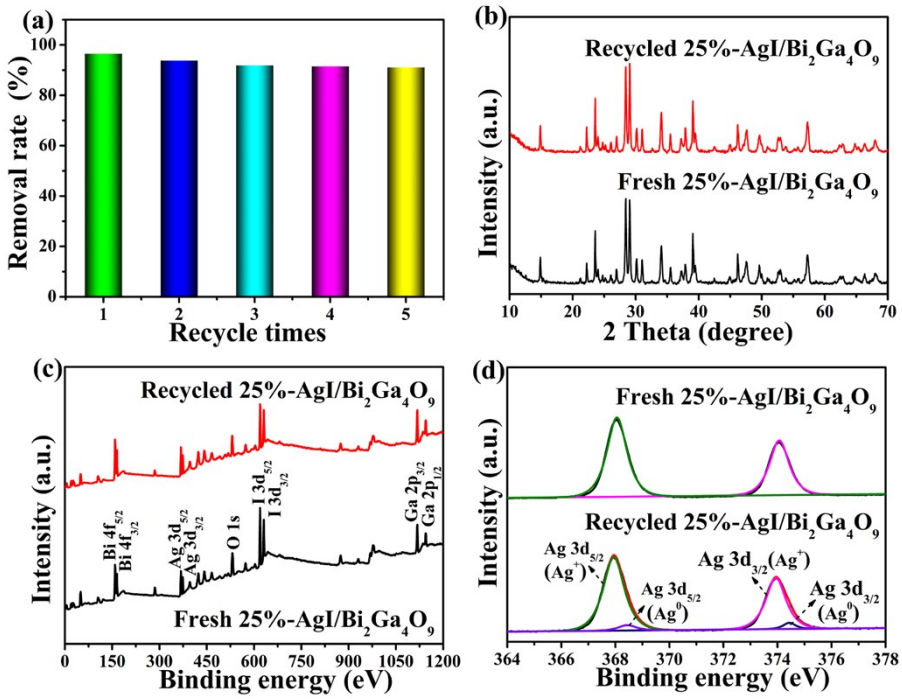

Fig. S10 (a) Recycling runs of 25%-AgI/$Bi_2Ga_4O_9$ for the photocatalytic degradation of AR1. (b) XRD patterns and (c) XPS survey spectra and (d) high resolution XPS Ag 3d spectra of the fresh and recycled 25%-AgI/$Bi_2Ga_4O_9$.

Table S1 The electrical properties of AgI sample.

Sample	Hall mobility ($m^2/V·s$)	Carrier concentration ($1/m^3$)	Hall coefficient (m^3/C)	Resistivity (Ω·m)	Hall voltage (V)	Conduction type
AgI	1.613×10^{-2}	1.919×10^{19}	0.325	20.165	2.681×10^{-3}	p